



Cite this: *Mater. Adv.*, 2022,
3, 2185

Preparation of heterostructured $\text{TiO}_2/\text{MoS}_2$ for efficient photocatalytic rhodamine B degradation†

Ping Li,‡^a Mengyou Gao,‡^{ab} Lei Sun,^a Huizhong Xu,^a Xiaochen Dong  ^c and Jianjian Lin  *^a

Coating a few layers of MoS_2 nanosheets on a substrate is an effective approach to enhance catalytic activity for photocatalytic degradation. Herein, we fabricated heterostructured $\text{TiO}_2/\text{MoS}_2$ ($\text{H-TiO}_2/\text{MoS}_2$) with high structural stability via a simple two-step solvothermal approach. $\text{H-TiO}_2/\text{MoS}_2$ was composed of TiO_2 as a hard core and MoS_2 nanosheets as a shell, which could increase the electron transfer rate between TiO_2 and MoS_2 and enable active edge sites of MoS_2 to be maximally exposed. Besides, $\text{H-TiO}_2/\text{MoS}_2$ indicated enhanced light absorption in the UV to Vis range when compared to TiO_2 nanoparticles, and slightly lower than that of MoS_2 . This is beneficial for the enhancement of the photocatalytic degradation performance. Therefore, $\text{H-TiO}_2/\text{MoS}_2$ displayed a strong adsorption ability toward organic dyes and showed excellent performance in the photocatalytic degradation of rhodamine B with the concentration decreased by 99.4% due to the synergistically stimulative effect. The work will enlighten the development of highly efficient molybdenum sulfide-based heterostructured photocatalysts.

Received 10th November 2021,
Accepted 9th January 2022

DOI: 10.1039/d1ma01050f

rsc.li/materials-advances

Introduction

Nowadays, semiconductor photocatalysts are attracting increasing attention owing to their high efficiency in easing the energy crisis and reducing environmental pollution. Recently, a large variety of semiconductor photocatalysts have been explored including TiO_2 ,^{1,2} SrTiO_3 ,³ *etc.*, which were mainly active in the ultraviolet range, and C_3N_4 ,⁴ Cu_2O , Co_3O_4 ,⁵ CdS ,⁶ *etc.* that have high visible light activity. TiO_2 , as an n-type photocatalytic semiconductor, is efficient for the separation of electrons and holes. Furthermore, it has both good chemical and physical stability, relatively low cost and nontoxicity, and thus has a wide range of applications in various fields, such as self-cleaning and removal of hazardous compounds. However, the large band gap of TiO_2 (3.2 eV) has become the main drawback because limited UV light could be used, which significantly decreased the photocatalytic performance. Additionally, pure TiO_2 usually did not have a high charge separation rate, and therefore illustrated relatively low

photocatalytic activity. Thus, many research studies have been conducted to settle these inadequacies including tuning the particle size,⁷ crystallinity and morphologies (nanotubes⁸ in 1D, nanosheets⁹ in 2D and microspheres¹⁰ or nanoflowers¹¹ in 3D), and constructing heterostructured materials,^{12–14} which have resulted in the promotion of the photocatalytic performance. Among these nanostructures, heterostructures like core–shell structures¹⁵ with a large specific surface area and matched energy levels have attracted great attention.

Moreover, it has been reported that TiO_2 -based photocatalysts doped with cocatalysts like noble metals,¹⁶ MoS_2 ,^{16–18} *etc.*, could broaden the range of light harvesting from the UV to UV-vis, and improve the charge separation efficiency. Two-dimensional transition metal sulfides (2D MS_x), such as the typical MoS_2 , were reported as platinum-like materials, which were beneficial for improving the photocatalytic performance as a cocatalyst because of great (photo) electronic and catalytic traits.¹⁹ In addition, a few-layered MoS_2 with increased edges was beneficial for electron acceptance, as well as increased active sites, illustrating improved photocatalytic performance. Recently, MoS_2 catalysts with a variety of nanostructures have been prepared using various approaches including chemical vapour deposition,²⁰ thermolysis²¹ or hydrothermal and solvothermal methods.²² Irregular aggregates of nanoparticles or stacked multilayers of the as-fabricated MoS_2 , however, largely limited the photocatalytic performance. Therefore, preparing heterostructured MoS_2 -based photocatalysts with enhanced photocatalytic activity remains challenging. Recently, MoS_2 -based photocatalysts such as CdS/MoS_2 ,^{23,24} graphene/

^a Shandong Key Laboratory of Biochemical Analysis, College of Chemistry and Molecular Engineering, Qingdao University of Science and Technology, Qingdao 266042, P. R. China. E-mail: Jianjian_Lin@qust.edu.cn

^b College of Automation and Electronic Engineering, Qingdao University of Science and Technology, Qingdao 266042, P. R. China

^c Key Laboratory of Flexible Electronics (KLOFE) & Institute of Advanced Materials (IAM), Nanjing Tech University (NanjingTech), 30 South Puzhu Road, Nanjing, 211800, P. R. China

† Electronic supplementary information (ESI) available. See DOI: 10.1039/d1ma01050f

‡ These authors equally contributed to this work



MoS_2 ^{25,26} and $\text{TiO}_2/\text{MoS}_2$ heterostructures with various structures including particles²⁷ (0D), belts²⁸ and wires¹² (1D), sheets²⁹ (2D) and flowers³⁰ (3D) have demonstrated enhanced photocatalytic activities. Meanwhile, constructing novel nanostructures of core-shelled $\text{TiO}_2/\text{MoS}_2$ is also an effective approach to develop photocatalysts with large specific surface areas and increased active sites.

In this work, we prepared H- $\text{TiO}_2/\text{MoS}_2$ through a two-step solvothermal approach. In the first step, TiO_2 nanoparticles were prepared as an ellipsoidal core through a solvothermal approach; then MoS_2 nanosheets were coated on the surface of the TiO_2 precursor again using a solvothermal method. The MoS_2 nanosheets which were coated on the surface of TiO_2 nanoparticles could allow fast electron transfer between TiO_2 and MoS_2 . Furthermore, H- $\text{TiO}_2/\text{MoS}_2$ illustrated good structural stability. MoS_2 nanosheets could expose active edge sites maximally, allowing an enhanced adsorption ability and improved photocatalytic degradation performance of rhodamine B (RhB). The synergistic effect of the novel heterostructure between MoS_2 nanosheets and TiO_2 nanoparticles accounted for the outstanding photocatalytic degradation performance.

Experimental

Chemicals

Tetrabutyl titanate (TBT, Aladdin Biochemical Technology Co., Ltd) and glacial acetic acid (Macklin Co., Ltd) were used without further purification. Absolute ethanol and $\text{Na}_2\text{MoO}_4 \cdot 2\text{H}_2\text{O}$ were purchased from Sinopharm Chemical Regent Co., Ltd. Cysteine was purchased from Beijing Xinjingke Biotechnology Co., Ltd. Ultrapure H_2O was employed in all experiments.

Preparation of TiO_2

In a typical synthesis process, the TiO_2 precursor was synthesized by a hydrothermal strategy.^{7,31} In detail, TBT (1 mL) was dropped into glacial acetic acid (15 mL) at room temperature, followed by addition of ultrapure water (0.3 mL) to initiate the hydrolysis of TBT. The mixture was stirred for ~10 minutes at room temperature, and then transferred into a 50 mL autoclave, which was heated at 150 °C for 12 h. The as-prepared precursor was obtained by centrifugation after cooling the autoclave to room temperature and washed thoroughly with absolute ethanol and water several times with the assistance of ultrasound treatment.

Synthesis of H- $\text{TiO}_2/\text{MoS}_2$

H- $\text{TiO}_2/\text{MoS}_2$ was prepared *via* a solvothermal method.²² In detail, 100 mg TiO_2 was dissolved into $\text{C}_2\text{H}_5\text{OH}$ (10 mL) and H_2O (20 mL), then $\text{Na}_2\text{MoO}_4 \cdot 2\text{H}_2\text{O}$ (0.3 g) and cysteine (1.25 g) were added under vigorous stirring in sequence. Then the mixed solution was transferred into an autoclave (50 mL) and heated at 200 °C for 24 h. The resultant sample was obtained by centrifugation after cooling the autoclave to room temperature. Finally, the obtained sample was washed thoroughly with

absolute ethanol and water several times with the assistance of ultrasound treatment. The as-fabricated H- $\text{TiO}_2/\text{MoS}_2$ was heated at 800 °C (5 °C min⁻¹) under an Ar (5% H_2) atmosphere for 2 h before collection.

Characterization

X-Ray diffraction (Bruker D8 Advance) with Ni-filtered Cu K α radiation was used to reveal the crystal structure of the as-prepared samples at 40 kV and 40 mA with a step size of 0.02° and scan speed of 0.1 s. Transmission electron microscopy (TEM, FEI Tecnai G2 F20) and scanning electron microscopy (SEM, Zeiss Merlin compact LE0 1530 VP) were used to explore the morphologies and elemental compositions of the as-prepared samples. The Raman spectrum of $\text{TiO}_2/\text{MoS}_2$ was recorded on an Invia Qontor. Fourier transform-infrared (FT-IR) spectroscopy was performed to confirm the spectrum of $\text{TiO}_2/\text{MoS}_2$ in the range of 400–4000 cm⁻¹ using a PerkinElmer Spectrum One spectrometer. N_2 adsorption and desorption curves were obtained for the analysis of pore structure by ASAP 2460. UV-Vis absorption spectra were recorded on a PerkinElmer (Lambda 1050 +) for revealing the light absorption of the as-prepared samples.

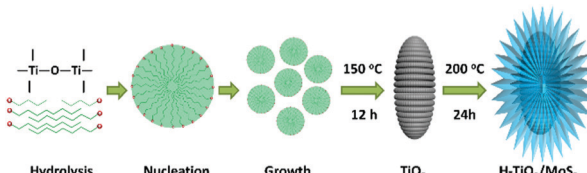
Photocatalytic degradation measurement

Photocatalytic activity was studied at room temperature by the degradation of RhB using a 300 W Xe lamp. For the photocatalytic test, 50 mL of an aqueous suspension of RhB (15 mg L⁻¹) and 5 mg of the samples were placed in a Pyrex glass tube. Before irradiation, the suspension was sonicated and stirred for 30 min in the dark. The mixed solution was continuously stirred during the photocatalytic reaction. During the photocatalytic reaction process, 3 mL of the suspension were collected after irradiation for the following analysis after the filtration. The concentration of RhB was monitored by measuring the absorbance at 554 nm using a UV-vis spectrometer (Lambda 1050 +). Isopropanol, DMSO and *t*-BuOH were used as free radical scavengers for the scavenging experiments. The pH values of RhB solution were controlled by 0.1 M HCl and 0.1 M NaOH.

Results and discussion

Morphology and composition

As illustrated in Scheme 1, H- $\text{TiO}_2/\text{MoS}_2$ was fabricated *via* a simple two-step method. Initially, the porous TiO_2 (rice-like) precursor was prepared *via* a facile solvothermal method;^{7,31} then the TiO_2 precursor was seen as a hard core, which loaded MoS_2 as a shell outside, resulting in the successful preparation of H- $\text{TiO}_2/\text{MoS}_2$. Firstly, the tetrabutyl titanate precursor was hydrolyzed and nucleated into TiO_2 microcrystals, and then the microcrystals gradually grew as porous TiO_2 . In detail, the tetrabutyl titanate precursor was hydrolyzed into numerous winding chain bundles after 2 h of reaction (Fig. S1a, ESI†). As the reaction proceeds, some chain bundles are gradually rotated and twisted into ellipsoidal aggregates which can serve as crystal nuclei.³¹ Finally, after 12 h of reaction, all the



Scheme 1 Scheme of the preparation process for as-prepared H-TiO₂/MoS₂.

ellipsoidal aggregates grew into ellipsoidal particles (Fig. S1b, ESI†). The H-TiO₂/MoS₂ heterostructure was formed by an L-cysteine-assisted method.^{22,32} For the self-assembly process of the H-TiO₂/MoS₂ heterostructure, the porous TiO₂ served as a precursor core for the adsorption of MoO₄²⁻ anions. When heated in the solution-phase reaction, L-cysteine can release H₂S, meanwhile acting as a sulfide source and a reducing agent.³² As the reaction time increased, H₂S *in situ* reacted with MoO₄²⁻ anions to form a two-dimensional nano-plate-like structure, which is common in other MoS₂-based composites.³³⁻³⁵ As illustrated in Fig. S2 (ESI†), MoS₂ can be loaded onto the surface of TiO₂ in a short time and gradually crystallize with time.

As shown in X-ray diffraction patterns of Fig. 1, the crystal structure of the as-prepared precursor can be confirmed as TiO₂ (anatase, Fig. S3a, ESI† JCPDS No. 21-1272).^{7,31} Besides, the crystal structure of the resultant sample was confirmed to be H-TiO₂/MoS₂, which corresponds to TiO₂ and MoS₂ (2H, Fig. S3b, ESI† JCPDS No. 37-1492)²² phases, indicating that H-TiO₂/MoS₂ was fabricated successfully.

To indicate the porous structure of TiO₂, the characterization studies including magnified SEM and TEM images and N₂ adsorption and desorption curves of a single TiO₂ particle were performed. As illustrated in Fig. S4a and b (ESI†), the SEM and TEM images showed that the TiO₂ particle had plenty of pores, and the N₂ adsorption and desorption curves demonstrated a specific surface area of 103.07 m² g⁻¹ for TiO₂ particles (Fig. S4c, ESI†).

The morphology of H-TiO₂/MoS₂ (~240 nm) was confirmed by SEM and TEM. The SEM image in Fig. 2a illustrated that MoS₂ nanosheets (~20 nm thickness) were coated on the surface of TiO₂ nanoparticles successfully, which matched well

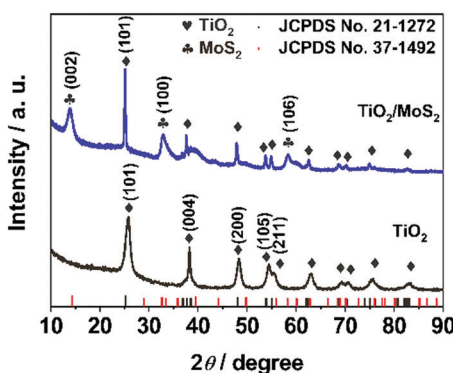


Fig. 1 XRD patterns of as-prepared TiO₂ and H-TiO₂/MoS₂.

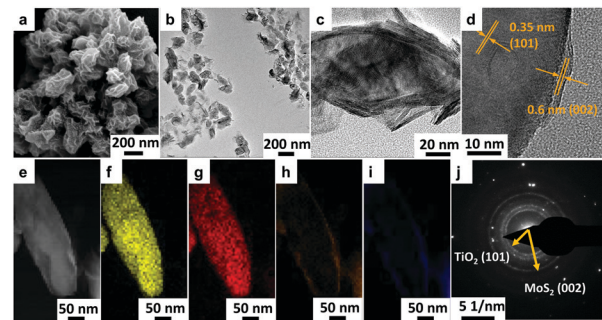


Fig. 2 (a) SEM, (b) low- and (c) high-magnification TEM image, (d) HRTEM image, (e–i) STEM EDS mapping images and (j) SAED image of H-TiO₂/MoS₂.

with the TEM image in Fig. 2b. Additionally, the single magnified particle in Fig. 2c clearly showed that a few layer MoS₂ (~10–30 layers) was loaded onto the surface of TiO₂. What is more, as illustrated in the high-resolution TEM (HRTEM) image of Fig. 2d, the lattice fringe of 0.35 nm corresponded to the (101) plane of TiO₂, and a lattice fringe of 0.6 nm corresponded to the (002) facet of MoS₂.³⁶ In order to explore the element dispersion of H-TiO₂/MoS₂, scanning transmission electron microscopy energy dispersive spectroscopy (STEM EDS) was employed. As shown in Fig. 2e–i, Ti and O were distributed evenly inside as a core, while Mo and S were located outside as a shell, demonstrating that MoS₂ encapsulated on the surface of TiO₂ successfully, which was consistent with SEM and TEM results.

Furthermore, the selected area electron diffraction (SAED) pattern in Fig. 2j pointed to the TiO₂ (101) facet and MoS₂ (002) facet, and corresponds well with the HRTEM image in Fig. 2d.

The rice-like morphology of the as-fabricated TiO₂ is clearly shown in Fig. 3a with ~200 nm in length and ~70 nm in width. Meanwhile, MoS₂ flowers were prepared and are shown in the SEM image in Fig. 3b.

The Raman scattering spectrum in Fig. 4a illustrated a series of Raman peaks of the as-prepared H-TiO₂/MoS₂, which corresponded to the typical peaks of MoS₂ and TiO₂. The peak located at 379 cm⁻¹ was attributed to the in-plane E_{2g}¹ mode, while the peak located at 404 cm⁻¹ was ascribed to the out-of-plane A_{1g} mode of MoS₂.³⁷ Meanwhile, the Raman peak located at 144 cm⁻¹ corresponded to the E_{1g} mode of TiO₂. The FT-IR spectrum of the as-prepared H-TiO₂/MoS₂ is shown in Fig. 4b. There are broad bands of H-TiO₂/MoS₂ at 486 cm⁻¹, 903 cm⁻¹, 1122 cm⁻¹, and 1640 cm⁻¹.³⁸ The band which was located at

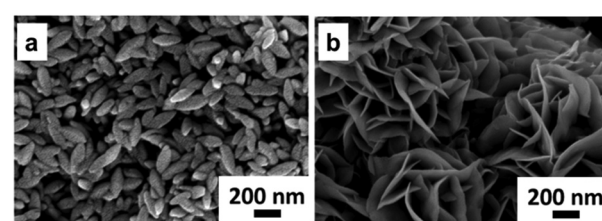
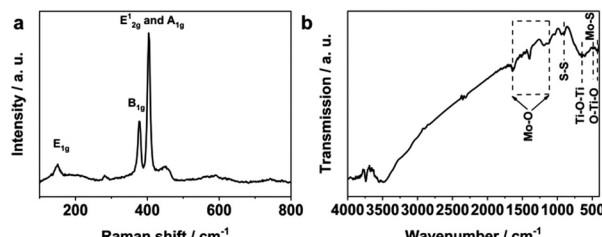


Fig. 3 SEM images of (a) TiO₂ nanoparticles and (b) MoS₂ flowers.



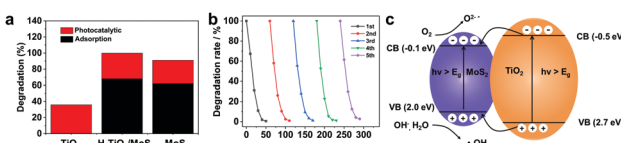
Fig. 4 Raman and FTIR spectra of as-prepared H-TiO₂/MoS₂.

486 cm⁻¹ corresponded to the Mo-S bond, while the band situated at 903 cm⁻¹ was assigned to the S-S bond. The bands between 1122 cm⁻¹ and 1640 cm⁻¹ were ascribed to the stretching vibrations of -OH and Mo-O.

Photo absorption and photocatalytic degradation of RhB

UV-Vis absorption spectra were obtained to understand the optical properties. As illustrated in Fig. S5 (ESI[†]), H-TiO₂/MoS₂ showed enhanced light absorption in the UV to Vis range when compared to TiO₂ nanoparticles, which is slightly lower than that of MoS₂. The photocatalytic degradation of RhB for H-TiO₂/MoS₂ was evaluated under a 300 W Xe lamp (Fig. 5a). Before light irradiation, the photocatalyst went through an adsorption process in RhB solution in the dark for 30 min. Interestingly, it is found that H-TiO₂/MoS₂ illustrated a stronger adsorption ability towards RhB than TiO₂ nanoparticles and MoS₂ flowers, which was reported have an efficient photocatalytic performance. In addition, the RhB photodegradation efficiency of H-TiO₂/MoS₂ was greater than that of TiO₂ nanoparticles and slightly higher than that of MoS₂ flowers, suggesting the advantages of H-TiO₂/MoS₂ nanostructures. Specifically, the concentrations of RhB were decreased by 32.6%, 36.2%, and 29.6% after irradiation with catalyst of H-TiO₂/MoS₂, TiO₂ nanoparticles, and MoS₂ flowers, respectively. It is remarkable that the concentration of RhB decreased by 99.4% using H-TiO₂/MoS₂, which was beneficial for RhB adsorption and degradation. As shown in Fig. 5b, the recycling stability of H-TiO₂/MoS₂ was tested for 5 cycles, and illustrated no evident decay, which demonstrated a good stability.

Additionally, as illustrated in Fig. S6 (ESI[†]), the consumed time for degradation decreased as the pH value increased. Specifically, it only took 20 min for RhB degradation at pH = 3, while it took ~50 min for RhB degradation at pH = 6.9 and 8.9. This indicated that the degradation of RhB was easier in acid solution.

Fig. 5 (a) Adsorption of RhB in dark (30 min) and photocatalytic degradation of RhB under the light irradiation (40 min) with TiO₂ nanoparticles, H-TiO₂/MoS₂ and MoS₂ flowers. (b) The recycling stability and (c) schematic photocatalytic degradation principle of H-TiO₂/MoS₂.

The schematic diagram (Fig. 5c) illustrates the energy band structure of H-TiO₂/MoS₂ and the process of electron transfer and the formation process of reactive oxygen species. Generally, the band gap of TiO₂ (anatase) was relatively wide (~3.2 eV), while the band gap of MoS₂ was narrower (~1.8 eV).³⁹ Upon light illumination, electrons could be excited from the valence band (VB) of MoS₂ to the conduction band (CB), leaving holes in the VB. Compared with TiO₂, it was easy to induce photo-generated electrons in MoS₂ with a relatively lower CB, and the photo-induced electrons (CB, MoS₂) could rapidly transport to TiO₂ nanoparticles (CB). The Mott-Schottky test was carried out to determine the flat-band potential of H-TiO₂/MoS₂.⁴⁰ As illustrated in Fig. S7 (ESI[†]), the potential can be confirmed to be ~-0.47 V (vs. SCE). The corresponding potential was converted to 0.18 V (vs. RHE) according to the equation E (vs. RHE) = E (vs. SCE) + 0.0591 pH + 0.244 V. Owing to dissolved oxygen in solution, photo-induced electrons could form superoxide radical anions from trapped O₂ (O₂ + e⁻ → O₂^{•-}), O₂^{•-}, as a high activity intermediate, usually used to degrade organic pollutants. On the valence band, the leaving holes were transferred from TiO₂ to MoS₂ due to the higher VB, H₂O was oxidized into hydroxyl radicals by holes with strong reduction (H₂O + h⁺ → OH[•]), which could oxidize organic dye into CO₂ and H₂O, etc.⁴¹ The active species generated in the process of photodegradation were h⁺, radical O₂[•] and radical OH[•].⁴² In order to reveal the main active species that played the significant role in the photodegradation of RhB, the free radical scavenging experiments were conducted. In detail, free radical scavengers of isopropanol, dimethylsulfoxide (DMSO) and t-BuOH were added to the photodegradation system as a h⁺ trapping agent, a radical O₂[•] trapping agent and a radical OH[•] trapping agent, respectively. As illustrated in Fig. S8 (ESI[†]), the photodegradation efficiency of RhB without adding a trapping agent was 94.7%, and the degradation efficiencies after adding isopropanol, t-BuOH and DMSO were 97.0%, 78.5% and 25.4%, respectively. The photodegradation performance of RhB was inhibited notably after adding DMSO, which confirmed that radical O₂[•] was the main active species used for oxidation and h⁺ played a synergistic role in the photocatalytic reaction,⁴³ and radical OH[•] indicated no evident effect.⁴⁴ H-TiO₂/MoS₂ was just tapping into its strong charge separation ability and weak charge-hole recombination ability for enhancing the photocatalytic degradation performance.

Conclusions

H-TiO₂/MoS₂ consisting of TiO₂ as a hard core and MoS₂ as a shell was prepared through a facile two-step solvothermal approach. H-TiO₂/MoS₂ was beneficial for fast electron transfer between TiO₂ and MoS₂ due to maximally exposed active edge sites of MoS₂ and illustrated high structural stability. Moreover, H-TiO₂/MoS₂ indicated enhanced light absorption and improved performance in the photocatalytic degradation of RhB (99.4%). The synergistic effect between MoS₂ nanosheets and TiO₂ nanoparticles accounted for the outstanding photocatalytic



degradation performance. Therefore, this novel photocatalyst is promising for preparing elaborate heterostructures and applications in various fields, such as sewage-treatment, dye degradation, *etc.*

Author contributions

Ping Li: data curation, writing – original draft, methodology, investigation. Mengyou Gao: supervision, writing – review and editing. Lei Sun: investigation, data curation. Huizhong Xu: data curation. Xiaochen Dong: methodology, investigation. Jianjian Lin: methodology, conceptualization, supervision, writing – review and editing.

Conflicts of interest

The authors declare that there are no conflicts to declare.

Acknowledgements

This work was partly supported by QUSTHX201919. J. Lin is supported by the Young Taishan Scholarship Project of Shandong Province (tsqn201909115).

Notes and references

- 1 A.-Y. Zhang, W.-Y. Wang, J.-J. Chen, C. Liu, Q.-X. Li, X. Zhang, W.-W. Li, Y. Si and H.-Q. Yu, Epitaxial Facet Junctions on TiO₂ Single Crystals for Efficient Photocatalytic Water Splitting, *Energy Environ. Sci.*, 2018, **11**, 1444–1448.
- 2 W. Zhang, H. He, Y. Tian, K. Lan, Q. Liu, C. Wang, Y. Liu, A. Elzatahry, R. Che, W. Li and D. Zhao, Synthesis of Uniform Ordered Mesoporous TiO₂ Microspheres with Controllable Phase Junctions for Efficient Solar Water Splitting, *Chem. Sci.*, 2019, **10**, 1664–1670.
- 3 L. Mu, Y. Zhao, A. Li, S. Wang, Z. Wang, J. Yang, Y. Wang, T. Liu, R. Chen, J. Zhu, F. Fan, R. Li and C. Li, Enhancing Charge Separation on High Symmetry SrTiO₃ Exposed with Anisotropic Facets for Photocatalytic Water Splitting, *Energy Environ. Sci.*, 2016, **9**, 2463–2469.
- 4 L. Ai, R. Shi, J. Yang, K. Zhang, T. Zhang and S. Lu, Efficient Combination of g-C₃N₄ and CDs for Enhanced Photocatalytic Performance: A Review of Synthesis, Strategies, and Applications, *Small*, 2021, 2007523.
- 5 L. Wang, J. Wan, Y. Zhao, N. Yang and D. Wang, Hollow Multi-Shelled Structures of Co₃O₄ Dodecahedron with Unique Crystal Orientation for Enhanced Photocatalytic CO₂ Reduction, *J. Am. Chem. Soc.*, 2019, **141**, 2238–2241.
- 6 R. Shen, D. Ren, Y. Ding, Y. Guan, Y. H. Ng, P. Zhang and X. Li, Nanostructured CdS for Efficient Photocatalytic H₂ Evolution: A Review, *Sci. China Mater.*, 2020, **63**, 2153–2188.
- 7 J. Lin, P. Li, H. Xu, Y. Kim, Z. Jing and D. Zheng, Controlled Synthesis of Mesoporous Single-Crystalline TiO₂ Nanoparticles for Efficient Photocatalytic H₂ Evolution, *J. Hazard. Mater.*, 2020, **391**, 122530.
- 8 P. Petrisková, O. Monfort, L. Satrapinský, E. Dobročka, T. Plecenik, G. Plesch, R. Papšík, R. Bermejo and Z. Lenčš, Preparation and Photocatalytic Activity of TiO₂ Nanotube Arrays Prepared on Transparent Spinel Substrate, *Ceram. Int.*, 2021, **47**, 12970–12980.
- 9 X. Tao, P. Ruan, X. Zhang, H. Sun and X. Zhou, Microsphere Assembly of TiO₂ Mesoporous Nanosheets with Highly Exposed (101) Facets and Application in a Light-Trapping Quasi-Solid-State Dye-Sensitized Solar Cell, *Nanoscale*, 2015, **7**, 3539–3547.
- 10 Z. Jiang, W. Wei, D. Mao, C. Chen, Y. Shi, X. Lv and J. Xie, Silver-Loaded Nitrogen-Doped Yolk-Shell Mesoporous TiO₂ Hollow Microspheres with Enhanced Visible Light Photocatalytic Activity, *Nanoscale*, 2015, **7**, 784–797.
- 11 Y. Liu, K. Lan, S. Li, Y. Liu, B. Kong, G. Wang, P. Zhang, R. Wang, H. He, Y. Ling, A. M. Al-Enizi, A. A. Elzatahry, Y. Cao, G. Chen and D. Zhao, Constructing Three-Dimensional Mesoporous Bouquet-Posy-like TiO₂ Superstructures with Radially Oriented Mesochannels and Single-Crystal Walls, *J. Am. Chem. Soc.*, 2017, **139**, 517–526.
- 12 X. Li, W. Li, M. Li, P. Cui, D. Chen, T. Gengenbach, L. Chu, H. Liu and G. Song, Glucose-Assisted Synthesis of the Hierarchical TiO₂ Nanowire@MoS₂ Nanosheet Nanocomposite and Its Synergistic Lithium Storage Performance, *J. Mater. Chem. A*, 2015, **3**, 2762–2769.
- 13 Y. Sun, H. Lin, C. Wang, Q. Wu, X. Wang and M. Yang, Morphology-Controlled Synthesis of TiO₂/MoS₂ Nanocomposites with Enhanced Visible-Light Photocatalytic Activity, *Inorg. Chem. Front.*, 2018, **5**, 145–152.
- 14 Q. Wang, P. Yu, L. Bai, R. Bao, N. Wang, C. Cheng, Z. Liu, M. Yang, W. Yang and Z. Guo, Self-Assembled Nano-Leaf/Vein Bionic Structure of TiO₂/MoS₂ Composites for Photoelectric Sensors, *Nanoscale*, 2017, **9**, 18194–18201.
- 15 R. Dai, A. Zhang, Z. Pan, A. M. Al-Enizi, A. A. Elzatahry, L. Hu and G. Zheng, Epitaxial Growth of Lattice-Mismatched Core-Shell TiO₂@MoS₂ for Enhanced Lithium-Ion Storage, *Small*, 2016, **12**, 2792–2799.
- 16 J. Liang, C. Wang, P. Zhao, Y. Wang, L. Ma, G. Zhu, Y. Hu, Z. Lu, Z. Xu, Y. Ma, T. Chen, Z. Tie, J. Liu and Z. Jin, Interface Engineering of Anchored Ultrathin TiO₂/MoS₂ Heterolayers for Highly-Efficient Electrochemical Hydrogen Production, *ACS Appl. Mater. Interfaces*, 2018, **10**, 6084–6089.
- 17 Q. Xiang, J. Yu and M. Jaroniec, Synergetic Effect of MoS₂ and Graphene as Cocatalysts for Enhanced Photocatalytic H₂ Production Activity of TiO₂ Nanoparticles, *J. Am. Chem. Soc.*, 2012, **134**, 6575–6578.
- 18 L. Zheng, S. Han, H. Liu, P. Yu and X. Fang, Hierarchical MoS₂ Nanosheet@TiO₂ Nanotube Array Composites with Enhanced Photocatalytic and Photocurrent Performances, *Small*, 2016, **12**, 1527–1536.
- 19 B. Chen, Y. Meng, J. Sha, C. Zhong, W. Hu and N. Zhao, Preparation of MoS₂/TiO₂ based Nanocomposites for Photocatalysis and Rechargeable Batteries: Progress, Challenges, and Perspective, *Nanoscale*, 2017, **10**, 34–68.
- 20 J. Zheng, X. Yan, Z. Lu, H. Qiu, G. Xu, X. Zhou, P. Wang, X. Pan, K. Liu and L. Jiao, High-Mobility Multilayered MoS₂



Flakes with Low Contact Resistance Grown by Chemical Vapor Deposition, *Adv. Mater.*, 2017, **29**, 1604540.

21 T.-Y. Chen, Y.-H. Chang, C.-L. Hsu, K.-H. Wei, C.-Y. Chiang and L.-J. Li, Comparative Study on MoS₂ and WS₂ for Electrocatalytic Water Splitting, *Int. J. Hydrogen Energy*, 2013, **38**, 12302–12309.

22 Q. Pang, Y. Zhao, X. Bian, Y. Ju, X. Wang, Y. Wei, B. Liu, F. Du, C. Wang and G. Chen, Hybrid Graphene@MoS₂@TiO₂ Microspheres for Use as a High Performance Negative Electrode Material for Lithium Ion Batteries, *J. Mater. Chem. A*, 2017, **5**, 3667–3674.

23 Y. Liu, H. Niu, W. Gu, X. Cai, B. Mao, D. Li and W. Shi, In situ Construction of Hierarchical CdS/MoS₂ Microboxes for Enhanced Visible-Light Photocatalytic H₂ Production, *Chem. Eng. J.*, 2018, **339**, 117–124.

24 L. Zhao, T. Dong, J. Du, H. Liu, H. Yuan, Y. Wang, J. Jia, H. Liu and W. Zhou, Synthesis of CdS/MoS₂ Nanoctaahedrons Heterostructure with a Tight Interface for Enhanced Photocatalytic H₂ Evolution and Biomass Upgrading, *Sol. RRL*, 2021, **5**, 2000415.

25 M. Yang, L. Wang, G. Hu, X. Chen, P. L. Gong, X. Cong, Y. Liu, Y. Yang, X. Li, X. Zhao and X. Liu, Optical Identification of Interlayer Coupling of Graphene/MoS₂ van der Waals Heterostructures, *Nano Res.*, 2021, **14**, 2241–2246.

26 W. Zhou, K. Zhou, D. Hou, X. Liu, G. Li, Y. Sang, H. Liu, L. Li and S. Chen, Three-Dimensional Hierarchical Frameworks Based on MoS₂ Nanosheets Self-Assembled on Graphene Oxide for Efficient Electrocatalytic Hydrogen Evolution, *ACS Appl. Mater. Interfaces*, 2014, **6**, 21534–21540.

27 X. Liu, Z. Xing, H. Zhang, W. Wang, Y. Zhang, Z. Li, X. Wu, X. Yu and W. Zhou, Fabrication of 3D Mesoporous Black TiO₂/MoS₂/TiO₂ Nanosheets for Visible-Light-Driven Photocatalysis, *ChemSusChem*, 2016, **9**, 1118–1124.

28 W. Zhou, Z. Yin, Y. Du, X. Huang, Z. Zeng, Z. Fan, H. Liu, J. Wang and H. Zhang, Synthesis of Few-Layer MoS₂ Nanosheet-Coated TiO₂ Nanobelt Heterostructures for Enhanced Photocatalytic Activities, *Small*, 2013, **9**, 140–147.

29 Y. Yuan, Z. Ye, H. Lu, B. Hu, Y. Li, D. Chen, J. Zhong, Z. Yu and Z. Zou, Constructing Anatase TiO₂ Nanosheets with Exposed (001) Facets/Layered MoS₂ Two-Dimensional Nanojunctions for Enhanced Solar Hydrogen Generation, *ACS Catal.*, 2015, **6**, 532–541.

30 K. He, Q. Wen, C. Wang, B. Wang, S. Yu, C. Hao and K. Chen, A Facile Synthesis of Hierarchical Flower-Like TiO₂ Wrapped with MoS₂ Sheets Nanostructure for Enhanced Electrorheological Activity, *Chem. Eng. J.*, 2018, **349**, 416–427.

31 J. Lin, L. Zhao, Y. Heo, L. Wang, F. Bijarbooneh, A. Mozer, A. Nattestad, Y. Yamauchi, S. Dou and J. Kim, Mesoporous Anatase Single Crystals for Efficient Co⁽²⁺³⁺⁾-Based Dye-Sensitized Solar Cells, *Nano Energy*, 2015, **11**, 557–567.

32 K. Chang and W. Chen, L-Cysteine-Assisted Synthesis of Layered MoS₂/Graphene Composites with Excellent Electrochemical Performances for Lithium Ion Batteries, *ACS Nano*, 2011, **5**, 4720–4728.

33 Q. Zhou, W. Li, M. Gao, H. Xu, Y. Guo, L. Sun, D. Zheng and J. Lin, A. Truncated Octahedron Metal-Organic Framework Derived TiO₂@C@MoS₂ Composite with Superior Lithium-Ion Storage Properties, *J. Power Sources*, 2022, **518**, 230746.

34 J. Yang, L. Yu, B. Zheng, N. Li, J. Xi and X. Qiu, Carbon Microtube Textile with MoS₂ Nanosheets Grown on Both Outer and Inner Walls as Multifunctional Interlayer for Lithium–Sulfur Batteries, *Adv. Sci.*, 2020, **7**, 1903260.

35 S. Wang, B. Guan, L. Yu and X. (David), Lou, Rational Design of Three-Layered TiO₂@Carbon@MoS₂ Hierarchical Nanotubes for Enhanced Lithium Storage, *Adv. Mater.*, 2017, **29**, 1702724.

36 J. Pei, H. Geng, E. H. Ang, L. Zhang, X. Cao, J. Zheng and H. Gu, Controlled Synthesis of Hollow C@TiO₂@MoS₂ Hierarchical Nanospheres for High-Performance Lithium-Ion Batteries, *Nanoscale*, 2018, **10**, 17327–17334.

37 B. Guo, K. Yu, H. Fu, Q. Hua, R. Qi, H. Li, H. Song, S. Guo and Z. Zhu, Firework-Shaped TiO₂ Microspheres Embedded with Few-Layer MoS₂ as an Anode Material for Excellent Performance Lithium-Ion Batteries, *J. Mater. Chem. A*, 2015, **3**, 6392–6401.

38 S. V. P. Vattikuti and C. Byon, Synthesis and Characterization of Molybdenum Disulfide Nanoflowers and Nanosheets: Nanotribology, *J. Nanomater.*, 2015, **2015**, 1–11.

39 X. Hu, H. Zhao, J. Tian, J. Gao, Y. Li and H. Cui, Synthesis of Few-Layer MoS₂ Nanosheets-Coated TiO₂ Nanosheets on Graphite Fibers for Enhanced Photocatalytic Properties, *Sol. Energy Mater. Sol. Cells*, 2017, **172**, 108–116.

40 Q. Zhang, Y. Wang, X. Zhu, X. Liu and H. Li, 1T and 2H Mixed Phase MoS₂ Nanobelts Coupled with Ti³⁺ Self-Doped TiO₂ Nanosheets for Enhanced Photocatalytic Degradation of RhB under Visible Light, *Appl. Surf. Sci.*, 2021, **556**, 149768.

41 H. Yan, L. Liu, R. Wang, W. Zhu, X. Ren, L. Luo, X. Zhang, S. Luo, X. Ai and J. Wang, Binary Composite MoS₂/TiO₂ Nanotube Arrays as a Recyclable and Efficient Photocatalyst for Solar Water Disinfection, *Chem. Eng. J.*, 2020, **401**, 126052.

42 Z. Li, F. Cao, L. Wang, Z. Chen and X. Ji, A Novel Ternary MoS₂/MoO₃/TiO₂ Composite for Fast Photocatalytic Degradation of Rhodamine B under Visible-Light Irradiation, *New J. Chem.*, 2020, **44**, 537–542.

43 D. Cao, Q. Wang, S. Zhu, X. Zhang, Y. Li, Y. Cui, Z. Xue and S. Gao, Hydrothermal Construction of Flower-Like MoS₂ on TiO₂ NTs for Highly Efficient Environmental Remediation and Photocatalytic Hydrogen Evolution, *Sep. Purif. Technol.*, 2021, **265**, 118463.

44 M. Mohamed and N. Karunakaran, One-Step Solvothermal Synthesis of Carbon Doped TiO₂–MoS₂ Heterostructure Composites with Improved Visible Light Catalytic Activity, *New J. Chem.*, 2016, **40**, 8123–8130.

